Establishing Metrics for Assessing the Performance of Directional Modulation Systems

Establishing Metrics for Assessing the Performance of Directional Modulation Systems

Yuan Ding, and Vincent Fusco, *Fellow, IEEE*

***Abstract*—In this paper metrics for assessing the performance of directional modulation (DM) physical-layer secure wireless systems are discussed. In the paper DM systems are shown to be categorized as static or dynamic. The behavior of each type of system is discussed for QPSK modulation. Besides EVM-like and BER metrics, secrecy rate as used in information theory community is also derived for the purpose of this QPSK DM system evaluation.**

***Index Terms*—Bit error rate, constellation pattern, directional modulation, error vector magnitude, secrecy rate.**

I. Introduction

Through the deployment of wireless networks we can readily acquire information and share data in real-time. However, this facility often comes at the expense of security due to the broadcast nature of wireless communications [1]. Traditionally the wireless secrecy problem has been handled at protocol stack level through mathematically derived cryptographic techniques. Physical-layer security, e.g., [2]-[4], has attracted research attention recently and suggests a means for achieving an additional level of security in a wireless transmission.

Physical-layer security exploits the unique physical properties of wireless communication channels in order to significantly reduce probability of successful data interception by eavesdroppers. A promising new concept termed directional modulation (DM) offers a means for achieving this. In a traditional beam-forming transmitter, information formats, i.e., constellation patterns in IQ space, are not distorted along undesired communication directions. Whereas in a DM transmitter, constellation patterns are spatially scrambled in all but an a-priori specified direction.

The authors in [5]-[7] introduced parasitic DM structures which rely on near-field coupling effects. In these cases the design process is complicated due to the complex interactions in the near-field and their spatial dependent transformation into the far-field. In contrast actively driven DM arrays [8]-[16] can be more synthesis-friendly since they allow linkage of array excitation settings to far-field patterns, and ultimately to the DM system performance. A further effort at simplifying DM architectures was made by exploiting the beam-orthogonality characteristics possessed by the Fourier transforming lens [17], [18]. More recently the artificial noise (orthogonal interference) [19], [20] and DM concepts were formally linked via the orthogonal vector approach in [21].

Since the DM technique is a relatively new concept, valid metrics to evaluate the performance of DM systems in a way that is consistent and which allows direct comparison between different systems have not been evolved. For example in [7], the authors only claimed that the DM properties were obtained by a certain physical arrangement, but no assessments were made. In [5], [6], [11]-[13] normalized error rate was adopted, however, since channel noise and coding strategy was not considered, this metric is not able to capture differences in performance if (a) a constellation symbol is constrained within its compartment, one quadrant for QPSK, but locates at different positions within that compartment; (b) a constellation symbol is out of its compartment but falls into a different compartment. In [17] an EVM-like figure of merit (FOM) for describing the capability of constellation pattern distortion in a DM system was defined. In [22] bit error rate (BER) was used to assess the performance of a QPSK DM system, but no information about how it is calculated was provided. While in [8], [9] a closed-form QPSK BER lower bound for DM system evaluation was proposed, which was recently corrected and extended in [14]. BER simulated via a random QPSK data stream was used in [9], [10], [15].

Additionally in DM system discussions there has not been adequate description of the effect that receive decoder properties has on system performance, especially in eavesdropper directions. Hence before BER results reported by various authors can be compared the influence of receive decoder capability needs to be described in details, as in [14]-[16], [18], [21].

To provide better cohesion in regard to DM system assessment comparability this paper brings together and contrasts available and newly proposed DM performance metrics. In Section II of this paper DM systems are categorized and are shown to be either static or dynamic based on whether the constellation distortion is updated, with respect to time, or not. An example QPSK DM transmitter for each type is presented and is used for DM metrics discussions later in the paper. In Section III and IV the possible metrics for static and dynamic QPSK DM systems are respectively presented, leaving metric discussions and comparisons as the topic of

Manuscript received July 29, 2013; revised Dec. 03, 2013. This work was sponsored by the Queen's University of Belfast High Frequency Research Scholarship.

Yuan Ding and Vincent Fusco are with the Institute of Electronics, Communications and Information Technology (ECIT), Queen's University of Belfast, Belfast, United Kingdom, BT3 9DT (phone: +44(0)2890971806; fax: +44(0)2890971702; e-mail: v.fusco@qub.ac.uk; yding03@qub.ac.uk).

Section V. Summaries are drawn in Section VI.

II. Static and Dynamic QPSK DM Systems

DM is a transmitter side technology that is able to scramble signal formats, i.e., constellation patterns in IQ space, along all spatial directions except for the direction pre-assigned for secure transmission.

Constellation distortion along unselected communication directions can be either constant during the entire transmission sequence, or it can be dynamically updated usually at the information symbol rate. From this point onwards, these are, respectively, termed static and dynamic DM systems.

A. Static DM systems

According to the definition above, DM architectures in [5]-[16], [22] are labeled the static DM systems.

A typical and synthesis-friendly static DM transmitter array is depicted in Fig. 1. Prior to transmission via N antenna elements, carrier signals (f_c) are modulated by baseband information data controlled attenuators with amplitude weights A_{mn} and phase shifters with values of $Phase_{mn}$, where m ($m = 1, 2, \ldots, M$) and n ($n = 1, 2, \ldots, N$) correspond to the m^{th} unique signal symbol and the n^{th} array element respectively. Usually this type of DM transmitter is synthesized by linking architecture parameter settings and the predicted system performance, then minimizing the values of appropriate cost functions via iterative optimization, as in [8], [14], [16].

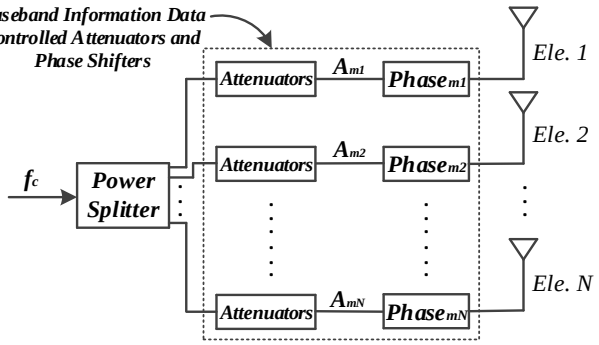

Fig. 1. A typical static DM transmitter array architecture, consisting of baseband information data controlled attenuators and phase shifters.

For the purpose of metric discussions in Section III, a static one-dimensional (1-D) half-wavelength spaced four-element DM transmitter array was synthesized with settings listed in Table I. It is modulated for QPSK with the selected secure communication direction of 150º (boresight is along 90º). The array elements are assumed to have ideal isotropic radiation patterns. The resulting far-field pattern for each QPSK symbol is presented in Fig. 2. These far-field patterns can also be regarded as constellation symbols in IQ space along each spatial direction. Gray coding is used throughout in this paper, thus the phase-synchronized symbols '11', '01', '00', and '10' in a standard QPSK system should lie in the first to the fourth quadrants respectively. For comparison the steering parameters for a conventional beam-steered QPSK transmitter pointing to 150º are also provided in Table I. Since in a conventional transmitter the signal is modulated at baseband, the $Phase_{mn}$ are fixed for each symbol transmitted, i.e., for each m. Fig. 2 shows the resulting far field patterns obtained for both DM and conventional array types. It is noted that for the conventional array type neither phase nor amplitude varies with transmitted

TABLE I
The Parameters of an Example QPSK DM Transmitter Array for 150º Direction Communication and Those of the Conventional Beam-Steering Array

DM QPSK transmitter array for 150º communication					
		***n*=1**	***n*=2**	***n*=3**	***n*=4**
***m*=1 (Symbol '11')**	A_{mn}	1.60	1.60	1.60	1.60
	$Phase_{mn}$	84º	194º	130º	240º
***m*=2 (Symbol '01')**	A_{mn}	1.47	1.47	1.47	1.47
	$Phase_{mn}$	91º	184º	267º	112º
***m*=3 (Symbol '00')**	A_{mn}	1.56	1.56	1.56	1.56
	$Phase_{mn}$	334º	139º	192º	344º
***m*=4 (Symbol '10')**	A_{mn}	1.60	1.60	1.60	1.60
	$Phase_{mn}$	231º	58º	121º	236º
Conventional beam-steering array pointing to 150º					
		***n*=1**	***n*=2**	***n*=3**	***n*=4**
(m = 1, 2, 3, 4)	A_{mn}	1	1	1	1
	$Phase_{mn}$	0º	204º	48º	252º

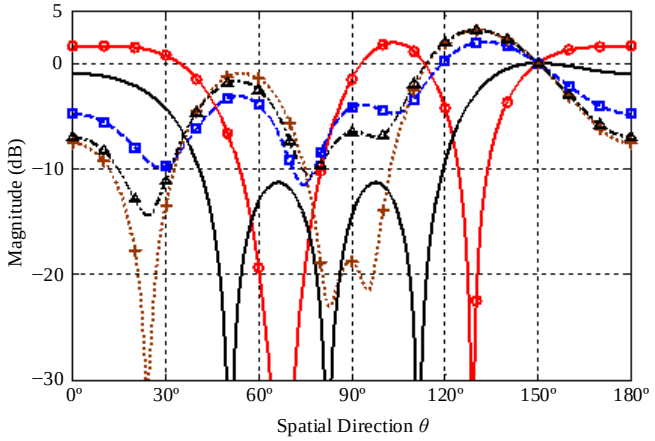

(a) Far-field magnitude patterns

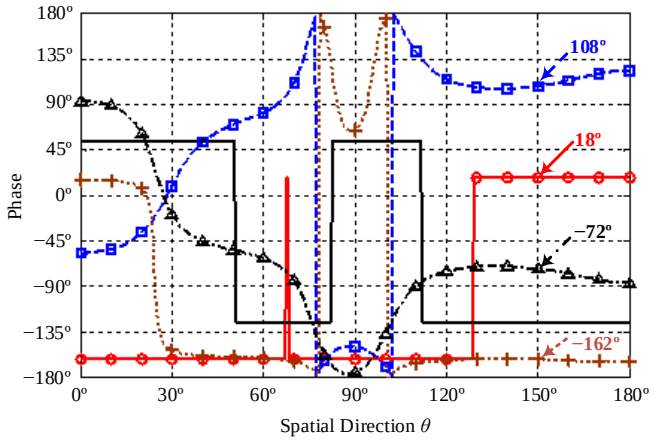

(b) Far-field phase patterns

Fig. 2. Far-field (a) magnitude and (b) phase patterns of the DM and the conventional arrays with the settings in Table I ('—o—': for symbol '11' in the DM array; '- -□- -': for symbol '01' in the DM array; '···+···': for symbol '00' in the DM array; '-·△-·': for symbol '10' in the DM array; '——': for four symbols in the conventional array).

symbol, whereas in the DM case they do with QPSK relative phase displacement and magnitude alignment occurring only along 150º. The reason of the far-field phase jumps of 180º for the conventional array as the power nulls are crossed is discussed in [23]. This is irrelevant to the phase distortion in DM arrays, which describes phase relations among modulated symbols.

B. *Dynamic DM systems*

When the constellation pattern distortions along other unselected spatial directions are randomly updated, usually at the information symbol rate, under the constraint that the standard modulation signal formats along the desired secure communication direction are well preserved, then the DM system is defined here as being dynamic. Dynamic DM can be achieved by updating either the array excitations [17], [18], [24] or the array element radiation patterns [25]. Dynamic DM systems perform better than static DM systems when eavesdroppers are equipped with sophisticated receivers [21].

The dynamic DM structures in [17], [18], [24], and [25] can be regarded as particular implementations of the orthogonal artificial interference concept [19]-[21]. Thus in this paper we take the general approach, i.e., dynamic DM transmitter array behavior is achieved by updating orthogonal artificial interference, for discussions in Section IV. Again we assume that the transmitter array consists of 1-D half-wavelength spaced antenna elements with isotropic radiation patterns, modulated for QPSK. Five array elements are used and 45º is selected as the desired secure communication direction.

To facilitate discussions the parameters and notations are provided below,

- The normalized channel vector along the desired direction θ_0, 45º in this example,

$$\vec{\boldsymbol{H}} = \frac{1}{\sqrt{5}} \cdot \left[e^{j2\pi\cos\theta_0} \quad e^{j\pi\cos\theta_0} \quad e^{j0} \quad e^{-j\pi\cos\theta_0} \quad e^{-j2\pi\cos\theta_0} \right]^T \quad (1)$$

  $[\,\bullet\,]^T$ refers to vector transpose operation;

- The normalized channel vectors along other unselected directions θ, $\theta \in [0º, 180º]$, $\theta \neq \theta_0$,

$$\vec{\boldsymbol{G}}(\theta) = \frac{1}{\sqrt{5}} \cdot \left[e^{j2\pi\cos\theta} \quad e^{j\pi\cos\theta} \quad e^{j0} \quad e^{-j\pi\cos\theta} \quad e^{-j2\pi\cos\theta} \right]^T \quad (2)$$

- The input excitation signal vector $\vec{\boldsymbol{S}}$,

$$\vec{\boldsymbol{S}} = \vec{\boldsymbol{H}}\boldsymbol{X} + \vec{\boldsymbol{W}} \quad (3)$$

  where $\boldsymbol{X}$ is a complex number representing the information symbol to be transmitted, e.g., $e^{j\pi/4}$ corresponds to the QPSK symbol '11'. $\vec{\boldsymbol{W}}$ is chosen to lie in the null space of $\vec{\boldsymbol{H}}^\dagger$. $(\,\bullet\,)^\dagger$ is the complex conjugate transpose (Hermitian) operation. Denote $\vec{\boldsymbol{Z}}_p$ (p = 1, 2, N-1) to be the orthonormal basis for the null space of $\vec{\boldsymbol{H}}^\dagger$, then $\vec{W} = \frac{1}{N-1} \cdot \sum_{p=1}^{N-1} \left(\vec{\boldsymbol{Z}}_p \cdot v_p \right)$.

  It is assumed that v_p has the same statistical distribution for each p.

Fig. 3 shows far-field patterns for 100 random QPSK symbols transmitted when the v_p are circularly symmetric i.i.d. (independent and identically distributed) complex Gaussian distributed variables with variance σ_v^2 of 0.8. The patterns are calculated by $\vec{\boldsymbol{H}}^\dagger \vec{\boldsymbol{S}}$ or $\vec{\boldsymbol{G}}^\dagger \vec{\boldsymbol{S}}$ for each direction.

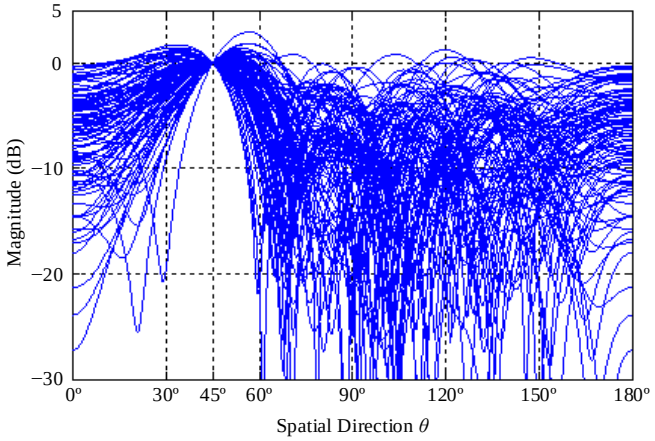

(a) Far-field magnitude patterns

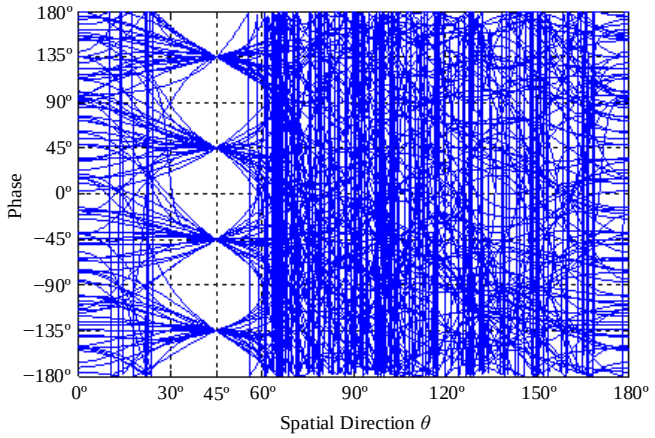

(b) Far-field phase patterns

Fig. 3. Far-field (a) power and (b) phase patterns of the dynamic QPSK DM transmitter array for 100 random QPSK symbols with circularly symmetric i.i.d. complex Gaussian distributed v_p (σ_v^2 = 0.8).

III. Possible Metrics for Assessing Static DM Systems

In this section possible metrics for assessing the performance of static DM systems are presented, and those for dynamic DM systems will be described in Section IV. The example static QPSK DM transmitter array presented in Section II part A with parameters in Table I is used throughout in this section.

A. *EVM-like Metrics*

In modern digital modulation communication systems error vector magnitude (EVM) is commonly adopted to quantify system performance because it can be calculated without demodulation and it also provides an insight in the physical origin of the distortion. Mathematically EVM can be expressed as [26]

$$EVM_{RMS} = \left[\frac{\frac{1}{T} \sum_{i=1}^{T} \left| S_{meas\_i} - S_{ref\_i} \right|^2}{\frac{1}{T} \sum_{i=1}^{T} \left| S_{ref\_i} \right|^2} \right]^{\frac{1}{2}} \quad (4)$$

where S_{meas_i} and S_{ref_i} are the i^{th} symbols in streams of measured and reference symbols in IQ space respectively, and T is the number of symbols transmitted.

In a non-DM system, i.e., a conventional system which refers to a transmitter consisting of baseband modulation, up-conversion and beam-steering via an antenna array, S_{ref} takes the value of the corresponding standard QPSK symbol. In such a case, EVM can be directly mapped to signal to noise ratio (SNR) and bit error rate (BER) [27].

When applying this EVM definition to the example static DM system and choosing S_{ref} along undesired spatial directions to be distorted symbols (S_{DM}), the EVM, denoted as EVM_{DM1}, is calculated and depicted in Fig. 4. The symbol stream length T is set to 10^6. The SNR, which is defined in a DM system as signal to AWGN power ratio along the desired communication direction, 150º in this example, is chosen to be 10 dB. The added power of AWGN is assumed to be identical along all directions. It is noted that in a DM system, SNR is no longer deterministically linked to EVM, thus it needs to be stated separately. For comparison, the EVM in the conventional system with the settings in Table I, denoted as EVM_{Conv} is also illustrated in Fig. 4.

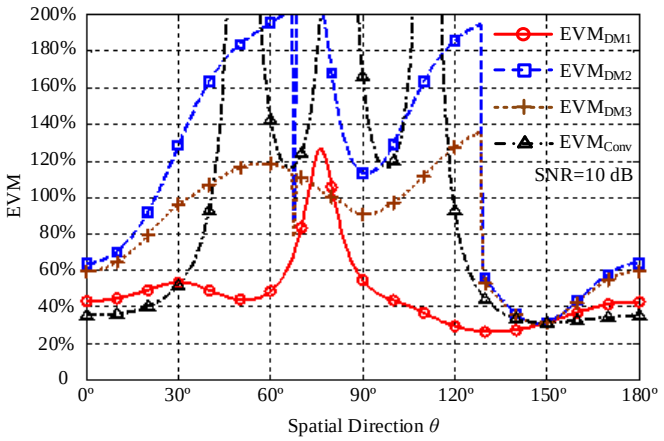

Fig. 4. The EVM_{DM} of the example static DM system and the EVM_{Conv} of the conventional system in Table I. SNR is set to 10 dB, and symbol length T is chosen to be 10^6.

With S_{ref} set to be noiseless but statically scrambled symbols (S_{DM}) the inherent distortions along unselected directions introduced by static DM systems are not involved. To allow their effects to be integrated with that of AWGN, we can set an imaginary standard QPSK constellation pattern along each spatial direction based on the same total received power of four unique QPSK symbols, namely $\sum_{j=1}^{4}\left|S_{ref\_j}\right|^2=\sum_{j=1}^{4}\left|S_{DM\_j}\right|^2$. Here we choose the phase of symbol '11' as phase reference. With these manipulations, the power normalized EVM with standard QPSK constellation reference, EVM_{DM2}, for the same static DM system is calculated and also shown in Fig. 4. This EVM_{DM2} is actually the FOM_{DM} defined in [17].

Besides getting imaginary standard QPSK constellation references based on the same total power criterion, we can alternatively generate references to maximize the signal to interference ratio (SIR) along each direction. Again the phase of symbol '11' is chosen as the phase reference. A distorted constellation pattern can be decomposed into a standard constellation pattern with an average symbol power P_e, which conveys the genuine information, and the interference with average power per symbol I_e^2, e.g., $I_e^2=\frac{1}{4}\left(\left|\boldsymbol{I}_{e1}\right|^2+\left|\boldsymbol{I}_{e2}\right|^2+\left|\boldsymbol{I}_{e3}\right|^2+\left|\boldsymbol{I}_{e4}\right|^2\right)$, see Fig. 5. The SIR is defined as P_e/I_e^2. For a given distorted constellation pattern, the separation can be arbitrary. However, the maximum value of SIR always exists, see Appendix. Take the pattern formed by S_{DM} in Fig. 5 as an example, the SIR_{max} of 8.64 is achieved when the $\sqrt{P_e}$ is chosen as 1.78, Fig. 6. This $\sqrt{P_e}$ can be used to set the length of the reference symbol, i.e., $|S_{ref}|$. The EVM with the SIR-maximized references, denoted as EVM_{DM3}, for the same static QPSK DM system is obtained and shown in Fig. 4.

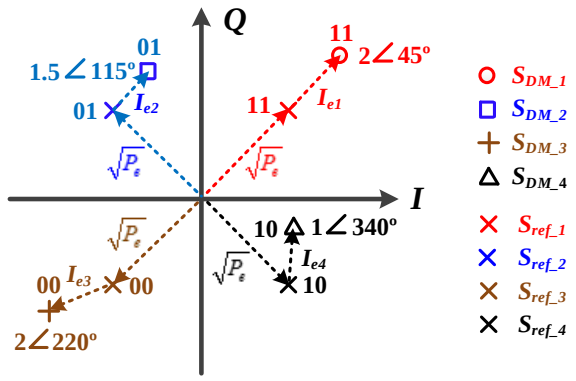

Fig. 5. Illustration of an example distorted pattern decomposition.

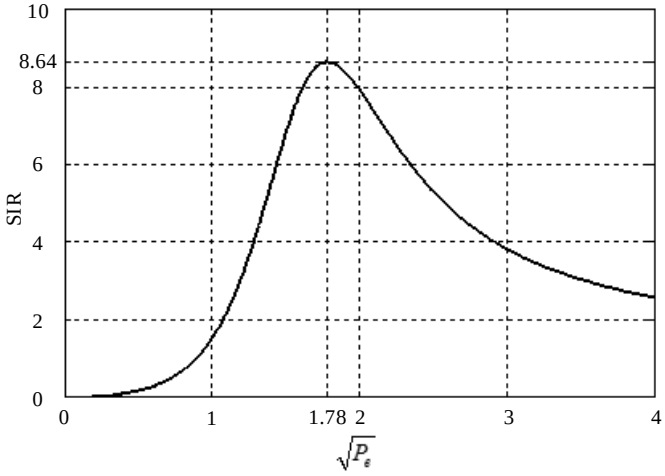

Fig. 6. SIR as a function of $\sqrt{P_e}$ for the example pattern in Fig. 5. The maximum SIR of 8.64 is achieved when $\sqrt{P_e}$ equals 1.78.

In order to gain more insights on the EVM-like metrics, the resulting EVM curves for the same static DM and conventional systems under higher SNR values of 20 dB and 100 dB (an extreme scenario equivalent to a noiseless wireless channel) are illustrated in Fig. 7 and Fig. 8, respectively. As expected, since the S_{ref} for the EVM_{DM2} and EVM_{DM3} calculations is chosen to be a standard QPSK constellation pattern, the inherent

distortion possessed by the static DM system dominates the system 'error vectors' at most directions. As a consequence, the EVM_{DM2} and EVM_{DM3} are insensitive to SNR, which describes the imperfection caused by channel noise, except in a small spatial region around the desired communication direction, where the inherent DM distortion disappears. On the other hand, the EVM_{DM1} and EVM_{Conv} are convergent to zero at all directions when SNR increases, as the S_{ref} choice for them makes AWGN channel noise the only source to the system 'error vectors'.

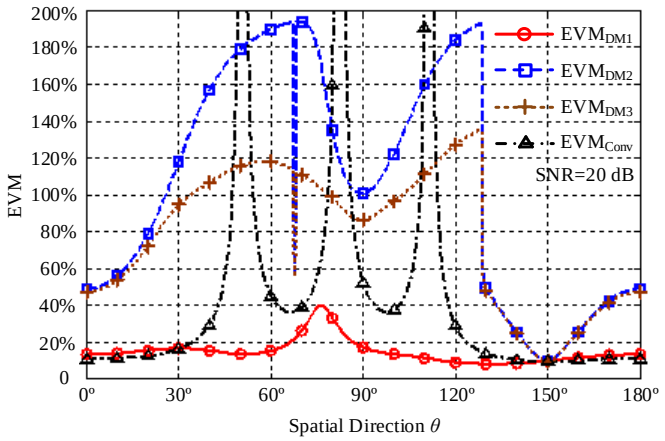

Fig. 7. The EVM_{DM} of the example static DM system and the EVM_{Conv} of the conventional system in Table I. SNR is set to 20 dB, and symbol length T is chosen to be 10^6.

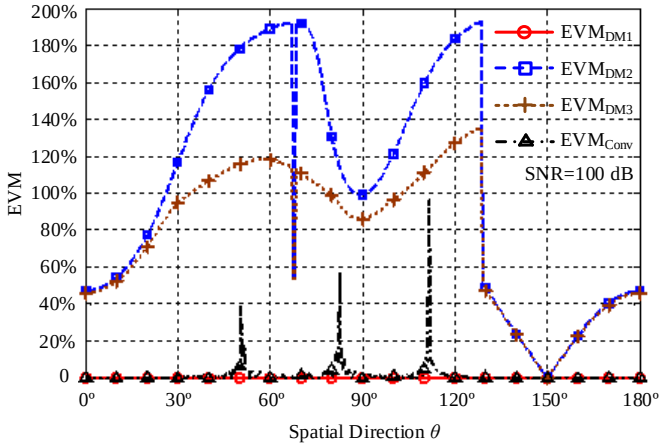

Fig. 8. The EVM_{DM} of the example static DM system and the EVM_{Conv} of the conventional system in Table I. SNR is set to 100 dB, and symbol length T is chosen to be 10^6.

B. BER Metrics

The BER criterion quantifies the effect of various distortions on the signals and, finally, on the recovered bit stream. Since receivers may have different capabilities to correct distortions, the same received signal can be differently decoded, resulting in different BER values. In other words, prior to BER calculations the receiver capabilities should be defined.

In this paper the authors propose the closed-form BER equations in (5) and (6) for static QPSK DM systems associated with, so called, APSK and QPSK type receivers. APSK receivers enable the 'minimum Euclidean distance decoding', while standard QPSK receivers decode received symbols based on which quadrant the constellation points locate into.

$$BER_{DM\_APSK} = \frac{1}{4}\cdot\sum_{i=1}^{4}\left[2^{k_i}\cdot Q\left(\sqrt{\frac{(d_i/2)^2}{N_0/2}}\right)\right] \tag{5}$$

$$BER_{DM\_QPSK} = \frac{1}{4}\cdot\left[\overbrace{Q\left(\sqrt{\frac{l_1^2\cdot sin^2(\pi/4)}{N_0/2}}\right)}^{Error_{11}} + Error_{01} + Error_{00} + Error_{10}\right] \tag{6}$$

Here $Q(\bullet)$ is the scaled complementary error function; d_i is the minimum distance between the i^{th} noiseless symbol (S_{DM_i}) with respect to any other noiseless symbols; k_i, the Gray code inspection coefficient, equals 0 (Gray code pair) or 1 (non-Gray code pair); $N_0/2$ is the noise power spectral density over a Gaussian channel; The $Error_{xy}$ can be obtained by $Q\left(\sqrt{\frac{l_i^2\cdot sin^2(\beta_i)}{N_0/2}}\right)$ (i = 2, 3, 4) when the noiseless symbol 'xy' is constrained within its quadrant. Parameter β_i is the minimum angle between the symbol vector (with the length l_i) and the decoding boundary, which overlaps the IQ axes. Otherwise 0.5 or 1 is assigned to $Error_{xy}$ depending on which quadrant this distorted noiseless symbol locates.

Using (5) and (6), we calculate the BER performance of the example static QPSK DM system under SNRs of 10 dB and 20 dB. These are shown in Fig. 9 and Fig. 10, where the BER curves for the conventional system are also illustrated for comparison. It can be noticed that the BER_{DM_APSK} and BER_{Conv} are scaled in all spatial directions as SNR varies, whereas the BER_{DM_QPSK} has the capability of retaining high BER values along most unselected communication directions, 30º to 130º in this example. This is due to the fact that the standard QPSK

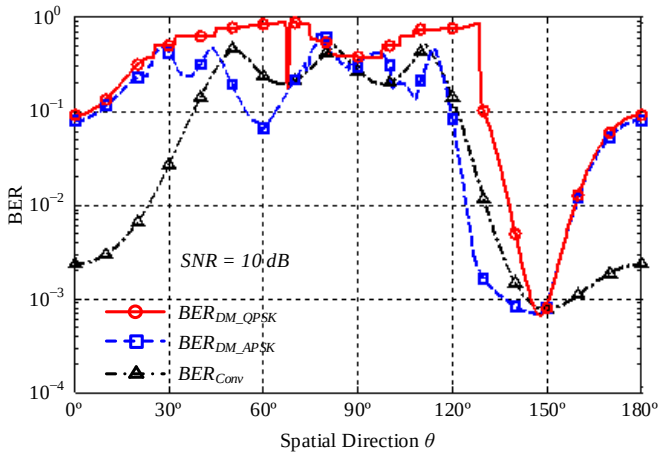

Fig. 9. BER spatial distributions calculated using the closed-form equations (5) and (6) for APSK and QPSK receiver types in the example static QPSK DM system and the conventional system. SNR is set to 10 dB. The BER spatial distributions calculated via a random symbol stream transmission in the static DM system approximately overlap their counterparts obtained by the closed-form equations.

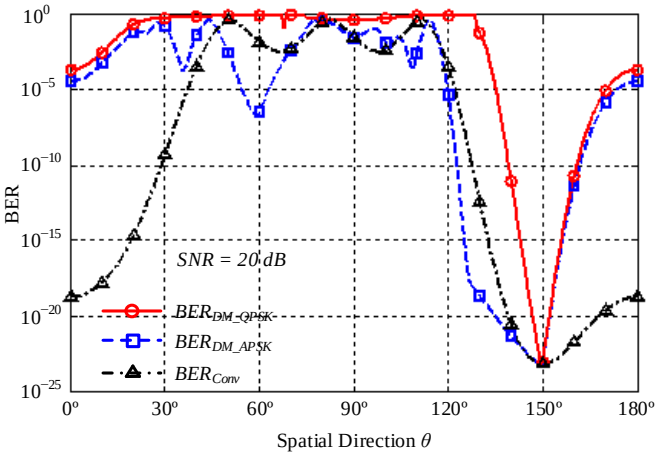

Fig. 10. BER spatial distributions calculated using the closed-form equations (5) and (6) for APSK and QPSK receiver types in the example static QPSK DM system and the conventional system. SNR is set to 20 dB. The BER spatial distributions calculated via a random symbol stream transmission in the static DM system approximately overlap their counterparts obtained by the closed-form equations for spatial region where BER is greater than 10^{-5}.

receiver cannot decode symbols located in non-designated quadrants correctly even when the channel is noise-free.

Instead of the closed-form approximations, BER for APSK and QPSK receivers can also be calculated via a random symbol stream transmission [17], [18], [21]. QPSK symbol streams with a length of 10^6 are used for simulation in this paper, which allows the BER down to 10^{-5} to be calculated. The simulated BER spatial distributions obtained by each method are virtually identical, Fig. 9 and Fig. 10.

C. Secrecy Rate Metrics

Research into information-theoretic security began with the wiretap channel model proposed by Wyner in 1975 [28]. The model and the analyses were generalized in [29], where the secrecy rate (R_{sec}) was defined as the difference in channel capacities between secure communication channels (C_m) and eavesdroppers' channels (C_e), (7). If the difference is negative, meaning eavesdroppers' channels have better quality, then R_{sec} is forced to zero. Operator $(x)^+$ returns zero if x is negative, otherwise x is returned.

$$R_{sec} = \left(C_m - C_e\right)^+ \tag{7}$$

In this paper we limit our discussions on transmissions of QPSK signals in free space, which is the case of discrete-time memoryless Gaussian channel with discrete input alphabets [30]-[34]. Thus instead of Shannon bound [35], [36] for the continuous input alphabets case, the channel capacity of the 4-ary modulation in AWGN channel [31] is adopted for secrecy rate calculations.

In a static QPSK DM system, let X, Y, and Z denote the transmitted discrete signal set, the signal detected by legitimate receiver, and the signals intercepted by eavesdroppers. Here X = $\{x_m \mid m = 1, 2, 3, 4\}$, corresponding to four unique QPSK symbols transmitted. The channel capacities over the secure communication channel (C_m) and over eavesdroppers' channels (C_e) for the QPSK systems can be calculated by finding maximum values of the mutual information between the transmitted signal X and the received signals, i.e., Y and Z respectively, and they are stated in (8) and (9).

$$C_m = max\,[\,I\,(\mathrm{X};\mathrm{Y})\,] \tag{8}$$

$$C_e = max\,[\,I\,(\mathrm{X};\mathrm{Z})\,] \tag{9}$$

In terms of (9), since the signals Z along undesired spatial directions are distorted not only by AWGN, but also by unique properties of DM systems, C_e over each potential eavesdropper's channel no longer follows the C_{QPSK} curve in Fig. 2 in [32]. Furthermore, SNR in these channels cannot be defined. The calculation of (9) is stated below. Here we assume that all transmitted constellation symbols are equally likely.

$$\begin{aligned}
C_e &= max\left[I\left(\mathrm{X};\mathrm{Z}\right)\right] \\
&= max\sum_{m=1}^{4}\left\{\int_{-\infty}^{\infty}\int_{-\infty}^{\infty} p\left(z\mid x_m\right)\cdot p\left(x_m\right)\cdot\log_2\left[\frac{p\left(z\mid x_m\right)}{p\left(z\right)}\right]\cdot dz_1\cdot dz_2\right\} \\
&= \sum_{m=1}^{4}\left\{\int_{-\infty}^{\infty}\int_{-\infty}^{\infty}\frac{1}{4}\cdot\prod_{r=1}^{2}\left[\frac{1}{\sqrt{\pi N_0}}\cdot e^{-\frac{\left(z_r-s_{mr}\right)^2}{N_0}}\right]\right. \\
&\qquad \left.\cdot\log_2\left(\frac{\prod_{r=1}^{2}\left[\frac{1}{\sqrt{\pi N_0}}\cdot e^{-\frac{\left(z_r-s_{mr}\right)^2}{N_0}}\right]}{\frac{1}{4}\cdot\sum_{u=1}^{4}\left\{\prod_{r=1}^{2}\left[\frac{1}{\sqrt{\pi N_0}}\cdot e^{-\frac{\left(z_r-s_{ur}\right)^2}{N_0}}\right]\right\}}\right)\cdot dz_1\cdot dz_2\right\} \\
&= \cdots \\
&= 2-\frac{1}{4\pi}\cdot\sum_{m=1}^{4}\left\{\overbrace{\int_{-\infty}^{\infty}\int_{-\infty}^{\infty} e^{-\left(t_1^2+t_2^2\right)}}^{K}\right. \\
&\qquad \left.\cdot\log_2\left[\sum_{u=1}^{4} e^{t_1^2+t_2^2-\left(t_1+\frac{s_{m1}-s_{u1}}{\sqrt{N_0}}\right)^2-\left(t_2+\frac{s_{m2}-s_{u2}}{\sqrt{N_0}}\right)^2}\right]\cdot dt_1\cdot dt_2\right\}
\end{aligned} \tag{10}$$

In (10) z_r is the I (for r = 1) or Q (for r = 2) components of the signal intercepted. s_{mr} (or s_{ur}) denotes the I (for r = 1) or Q (for r = 2) components of the noiseless but distorted signal for the m^{th} (or u^{th}) unique QPSK symbol, i.e., S_{DM} mentioned in Part A this section. t_1 and t_2 are new integration variables. The two-fold integral K in (10) can be numerically approximated using the products of the Gaussian-Hermite quadrature [37], [38]. In this paper the integration point number of 16 is used for K calculations. Applying (10) we obtain the channel capacity along each spatial direction in the example static QPSK DM system for the SNR of 10 dB. From this the secrecy rate spatial

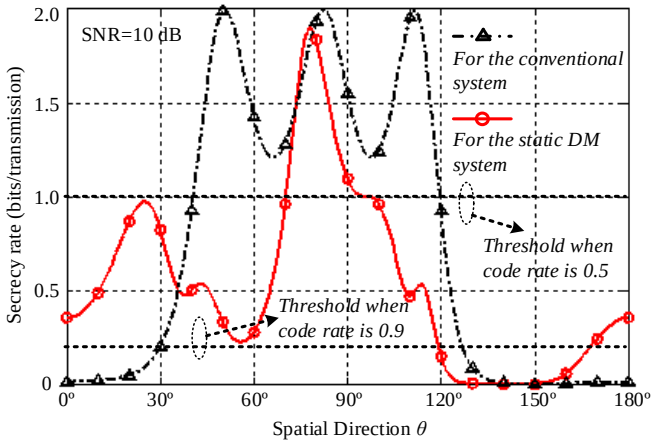

Fig. 11. Secrecy rate (bits/transmission) spatial distributions for the example static QPSK DM system and the conventional system. SNR is set to 10 dB along the desired communication direction, 150°. The decodable thresholds, discussed in Section V, for code rates of 0.5 and 0.9 are provided.

distributions can be calculated using (7), Fig. 11. The secrecy rate curve obtained for the conventional QPSK system is also shown for comparison. To confirm the calculations using (10) a bit-wise computation of mutual information was performed [39]. When the transmitted QPSK constellation symbols are well formatted, the resulting channel capacity values are identical to their counterparts calculated by (10). However, if constellation patterns are significantly distorted, the probability density function fittings, involved in the bit-wise method, can introduce more errors than the numerical integration of (10). Thus we choose (10) to calculate the channel capacity, and hence the secrecy rate in this paper. Under higher SNR scenarios, the secrecy rates for the DM and the conventional cases are convergent to zero at all directions except the three discrete power null directions for the conventional array, which are similar to EVM_{DM1} and EVM_{Conv} curves in Fig. 8.

IV. Possible Metrics for Assessing Dynamic DM Systems

Next possible metrics for assessing the performance of dynamic DM systems are presented below. The example dynamic QPSK DM transmitter array in Section II part B is used throughout in this section. The conventional system in this section refers to the 1-D half-wavelength spaced 5-element array with main beam steered to the selected communication direction of 45°. It is equivalent to the example dynamic DM system with a variance σ_v^2 of zero.

A. EVM-like Metrics

The EVM definition for dynamic DM systems is the same as that for static ones, (4). Since the orthogonal artificial interference injected into the example dynamic QPSK DM system has a distribution with zero-mean, three S_{ref} choices, which are averaged noiseless symbols S_{DM}, the total power normalized standard QPSK symbols, and the SIR-maximized standard QPSK symbols, are identical, resulting in overlaps of EVM_{DM1}, EVM_{DM2}, and EVM_{DM3}. They are illustrated in Fig. 12 and Fig. 13, respectively, for SNRs of 10 dB and 20 dB. As expected, EVM_{DM} is less sensitive to the channel noise along directions away from the selected communication direction, compared with EVM_{Conv} in the conventional system.

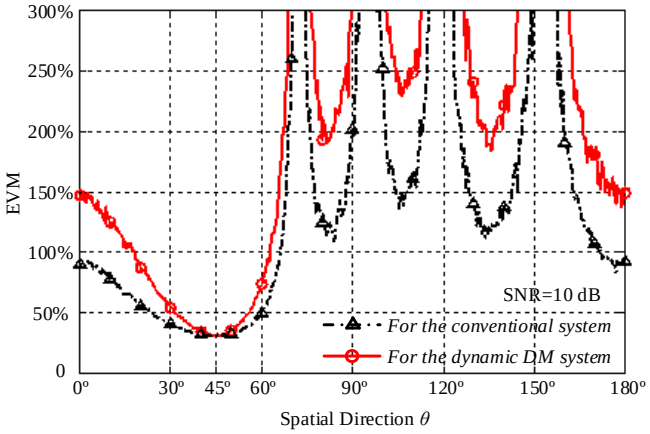

Fig. 12. The EVM_{DM} of the example dynamic DM system and the EVM_{Conv} of the conventional system. The EVM_{DM1}, EVM_{DM2}, and EVM_{DM3} overlap each other. SNR is set to 10 dB, and symbol length T is chosen to be 10^6.

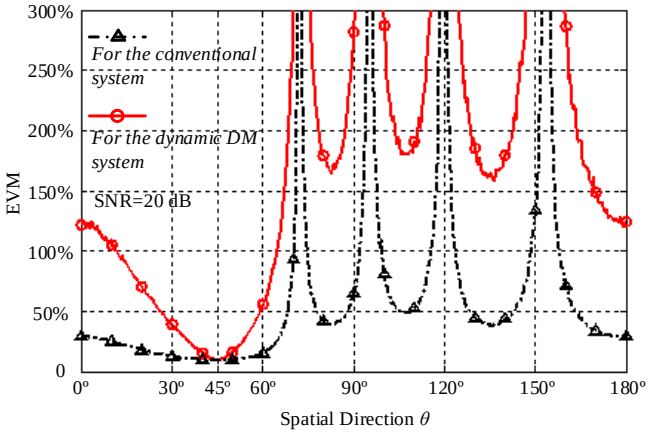

Fig. 13. The EVM_{DM} of the example dynamic DM system and the EVM_{Conv} of the conventional system. The EVM_{DM1}, EVM_{DM2}, and EVM_{DM3} overlap each other. SNR is set to 20 dB, and symbol length T is chosen to be 10^6.

B. BER Metrics

Since the orthogonal artificial interference in the example dynamic DM system has Gaussian distribution, its effect on BER can be integrated with that of the AWGN. As a consequence the closed-form BER equations for the APSK and QPSK receiver types can be readily derived by replacing N_0 with $N_0+\frac{\sigma_v^2}{N-1}\left(\bar{\boldsymbol{G}}^\dagger\bar{\boldsymbol{Z}}\bar{\boldsymbol{Z}}^\dagger\bar{\boldsymbol{G}}\right)$ in (5) and (6). With these manipulations, the BER spatial distributions are calculated by the closed-form equations, and are shown in Fig. 14 and Fig. 15 for SNRs of 10 dB and 20 dB. Again the zero-mean property of the artificial interference distribution makes BER curves for APSK and QPSK receiver types identical. Under both SNR scenarios the BERs simulated by transmitting a 10^6 random QPSK data stream are also presented.

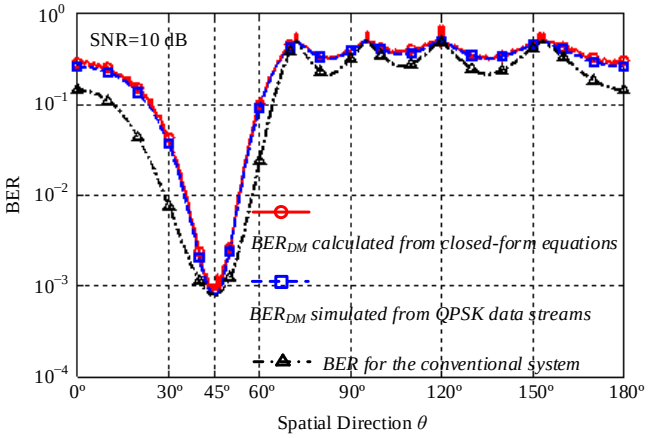

Fig. 14. The BER_{DM} of the example dynamic DM system obtained from both the closed-form equations and random QPSK data streams, and the BER of the conventional system. The BER_{DM_APSK} and BER_{DM_QPSK} overlap each other. SNR is set to 10 dB, and symbol length T is chosen to be 10^6.

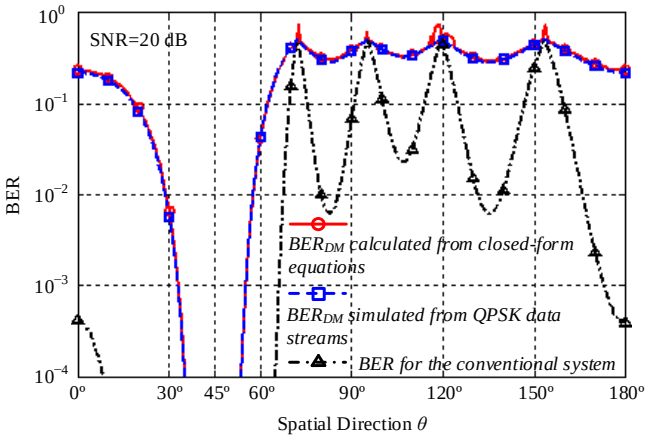

Fig. 15. The BER_{DM} of the example dynamic DM system obtained from both the closed-form equations and random QPSK data streams, and the BER of the conventional system. The BER_{DM_APSK} and BER_{DM_QPSK} overlap each other. SNR is set to 20 dB, and symbol length T is chosen to be 10^6.

C. Secrecy Rate Metrics

Similarly by replacing N_0 with $N_0+\frac{\sigma_v^2}{N-1}\left(\vec{G}^{\dagger}\vec{Z}\vec{Z}^{\dagger}\vec{G}\right)$ in (10), the channel capacity spatial distribution for QPSK modulation can be calculated, which results in the secrecy rate of the example dynamic QPSK DM system via (7), Fig. 16. SNR is set to 10 dB along the desired communication direction, 45º. For higher SNR, two curves are inevitably converged to zero except four discrete power null directions.

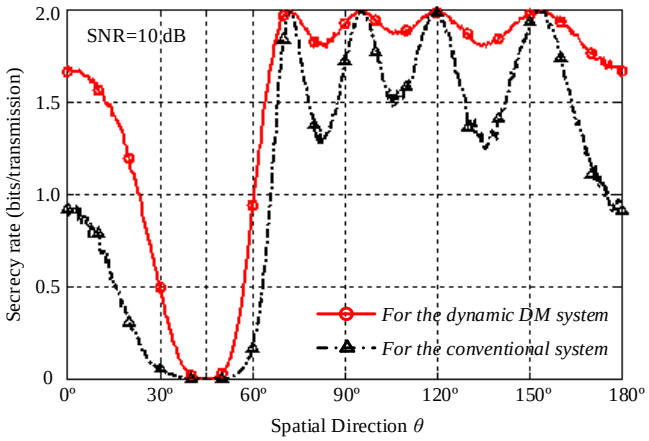

Fig. 16. Secrecy rate (bits/transmission) spatial distributions for the example dynamic QPSK DM system and the conventional system. SNR is set to 10 dB along the desired communication direction, 45º.

V. Metrics Discussions and Comparisons

In this section, we analyze the possible metrics for DM systems presented in Section III and IV, and make comparisons among them.

A. Metrics for Static DM Systems

Firstly, BERs calculated from the closed-form equations and random QPSK data streams resemble each other.

If we still use the relationship between EVM and BER stated in [27], although we acknowledge that the relationship does not hold for static DM systems, the calculated BER_{DM1}, BER_{DM2}, and BER_{DM3}, corresponding to the EVM_{DM1}, EVM_{DM2}, and EVM_{DM3} respectively, are illustrated in Fig. 17, together with BER curves calculated via a random symbol stream. It can be observed that BER_{DM1} can roughly predict the spatial directions of the ripples on the BER_{DM_APSK} curve because the same symbol references, S_{DM}, are used. However, a discrepancy of around 10^2 along undesired directions makes the BER_{DM1} unusable. Although the BER_{DM2} and BER_{DM3} are approximate predictions of the BER_{DM_QPSK} curve, compared with the closed-form BER method, they are neither precise nor calculation-friendly.

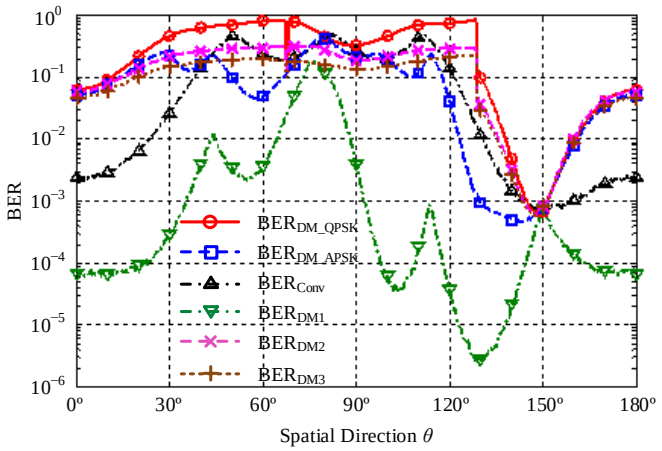

Fig. 17. The BER_{DM1}, BER_{DM2}, and BER_{DM3}, calculated from the EVM_{DM1}, EVM_{DM2}, and EVM_{DM3} respectively, and the BER curves calculated via a random symbol stream. SNR is set to 10 dB along 150º, and symbol length T is chosen to be 10^6.

At first glance the results in Fig. 11 tell us that the secrecy performance of the conventional system is generally better. However, the conclusion cannot be drawn before setting a threshold, which is determined by modulation scheme and the rate of the code. The code rate is defined as the number of message bits per data bit. For example, if the transmitted signal is modulated with QPSK, which has 4 symbols and thus 2 bits per symbol, and the code rate chosen is 0.9, then 2×0.9=1.8 message bits are conveyed per channel use. When the capacity

of a channel for QPSK input is greater than 1.8 bits per transmission, the receiver is able to recover the information with arbitrarily low error. Otherwise, it would suffer a low probability of decoding any data. When considering (7), the threshold of the secrecy rate for the QPSK modulation scheme is C_m – (code rate)×2. We label the spatial directions with secrecy rate lower than the threshold as decodable region. For the example static QPSK DM system, if the code rate is chosen to be 0.5, then the threshold for the secrecy rate in Fig. 11 is $C_m - 0.5\times2 = 1.99 - 1 \approx 1$ bit per transmission when SNR is 10 dB. As a consequence, the conventional system outperforms the static DM system since it owns wider spatial range where potential eavesdroppers cannot recover the encoded information, i.e., the decodable region in the conventional system is smaller. When we increase the code rate to 0.9, the opposite conclusion is obtained since the threshold for the secrecy rate is $C_m - 0.9\times2 \approx 0.2$ bit per transmission. In fact the secrecy rate and the $\text{BER}_{\text{DM\_APSK}}$ can be mapped onto each other by eliminating the parameter N_0 in (5) and (10). A distribution similarity between them can be observed in Fig. 9 and Fig. 11. However, the secrecy rate representation provides guidelines for choosing code rates in various system scenarios.

B. Metrics for dynamic DM Systems

In Fig. 14 and Fig. 15, it can be seen that BER curves calculated from the closed-form equations and random QPSK data streams overlap each other, which can also be predicted by EVM_{DM} in Fig. 12 and 13, respectively, since the injected orthogonal artificial interference has zero-mean Gaussian distribution in the example dynamic QPSK DM system. Thus in this type of case EVM_{DM} is a suitable metric to evaluate system performance without data decoding. However, in a real transmitter where the linear and dynamic range is limited, Gaussian distributed orthogonal artificial interference is impossible, e.g., the dynamic DM systems reported in [17] and [21] generated the orthogonal interference with constant magnitudes. As a consequence, the EVM_{DM} fails to provide much information about the system performance. Furthermore

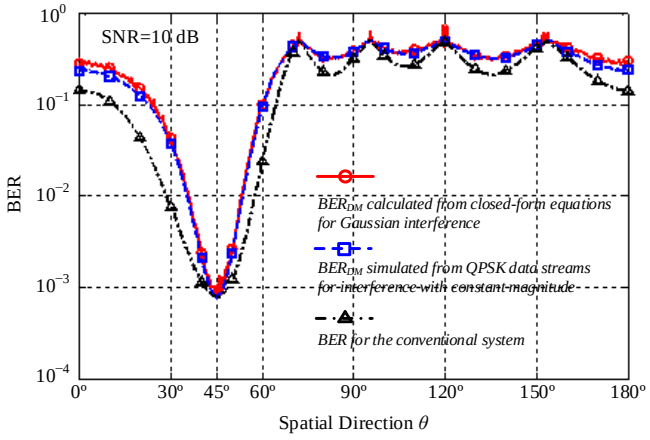

Fig. 18. The BER_{DM} simulated from QPSK data streams for interference with constant magnitude and that obtained from the closed-form BER equations for Gaussian interference. The interference power is the same. SNR along 45° is set to 10 dB.

closed-form BER and secrecy rate calculations are not available. Under the constraint of the same power, Gaussian distributed noise or interference is the worst case for decoding [40], thus the BER and secrecy rate obtained from the closed-form equations for Gaussian distributed orthogonal interference can be regarded as their achievable upper bounds, respectively. In Fig. 18 the BER for a dynamic QPSK DM system with constant magnitude orthogonal artificial interference is depicted. The interference power is the same as that for Gaussian distributed interference with the variance σ_v^2 of 0.8.

VI. Conclusion

Metrics for assessing the performance of DM systems were provided in this paper. It was shown that for static DM systems BER, calculated from either closed-form equations or random data streams, and secrecy rate were applicable for system performance evaluation, whereas EVM-like metrics did not perform well. For dynamic DM systems under the scenarios of zero-mean Gaussian distributed orthogonal interference, EVM-like metrics, BER, and secrecy rate were equivalent and can be converted into each other. For other interference distributions no closed-form BER and secrecy rate equations were available. The work in this paper can act as an assessment guideline for future DM system evaluation and cross system comparison.

Appendix

In this Appendix, we briefly prove that for a given distorted DM QPSK constellation pattern, the maximum value of SIR, defined in Section III part A, always exists.

$$\text{SIR} = \frac{P_e}{I_e^2} = \frac{4P_e}{I_1^2 + I_2^2 + I_3^2 + I_4^2}$$

$$= \frac{4P_e}{\left|S_{DM\_1} - S_{ref\_1}\right|^2 + \left|S_{DM\_2} - S_{ref\_2}\right|^2 + \left|S_{DM\_3} - S_{ref\_3}\right|^2 + \left|S_{DM\_4} - S_{ref\_4}\right|^2} \quad \text{(A1)}$$

In (A1), S_{DM_n} (n = 1, 2, 3, 4) are the four QPSK symbols in IQ space in a static DM system along a certain unselected spatial direction, and S_{ref_n} (n = 1, 2, 3, 4) are imaginary standard QPSK constellation. The phase of symbol '11' is chosen as the phase reference. Thus,

$$S_{DM\_1} = k \cdot S_{ref\_1} \quad \text{(A2)}$$

$$\left|S_{ref\_1}\right| = \left|S_{ref\_2}\right| = \left|S_{ref\_3}\right| = \left|S_{ref\_4}\right| = \sqrt{P_e} \quad \text{(A3)}$$

$$S_{ref\_n} = S_{ref\_1} \cdot e^{j(n-1)\pi/2} \qquad (n = 2,\ 3,\ 4) \quad \text{(A4)}$$

$$S_{DM\_n} = c_n \cdot S_{DM\_1} \qquad (n = 2,\ 3,\ 4) \quad \text{(A5)}$$

k is a real number ranging from 0 to infinite, and c_n are complex constants. From (A1) to (A5), we can derive that

$$\begin{aligned}\frac{4}{\mathrm{SIR}} &= (k-1)^2 + \left|k\cdot c_2 - e^{j\pi/2}\right|^2 + \left|k\cdot c_3 - e^{j\pi}\right|^2 + \left|k\cdot c_3 - e^{j3\pi/2}\right|^2 \\ &= k^2 - 2k + 1 + \\ &\quad |c_2|^2\cdot k^2 - 2|c_2|\cdot k\cdot\cos(\alpha_2) + 1 + \\ &\quad |c_3|^2\cdot k^2 - 2|c_3|\cdot k\cdot\cos(\alpha_3) + 1 + \\ &\quad |c_4|^2\cdot k^2 - 2|c_4|\cdot k\cdot\cos(\alpha_4) + 1 \\ &= a\cdot k^2 + b\cdot k + 4\end{aligned} \tag{A6}$$

α_n (n = 2, 3, 4) is the angle between c_n and $e^{j(n-1)\pi/2}$. Since

$$a = 1 + |c_2|^2 + |c_3|^2 + |c_4|^2 > 0 \tag{A7}$$

The minimum value of $\frac{4}{\mathrm{SIR}}$ exists when k belongs to $(0, +\infty)$. In other words, the maximum value of SIR always exists. The corresponding value of $\sqrt{P_e}$, with which the maximum SIR is reached, can be obtained via (A2) and (A3).

ACKNOWLEDGMENT

The authors would like to thank Dr. Youngwook Ko for useful discussions. They would also like to thank the anonymous reviewers and editors for their valuable comments and suggestions.

REFERENCES

[1] X. Li, J. Hwu, and E. P. Ratazzi, "Using antenna array redundancy and channel diversity for secure wireless transmissions," *Journal of Communications*, vol. 2, no. 3, pp. 24–32, May 2007.

[2] Y. Hwang and H. C. Papadopoulos, "Physical-layer secrecy in AWGN via a class of chaotic DS/SS systems: analysis and design," *IEEE Trans. Signal Processing*, vol. 52, no. 9, pp. 2637–2649, Sept. 2004.

[3] Yi-Sheng Shiu, Shih-Yu Chang, Hsiao-Chun Wu, S. C. Huang, and Hsiao-Hwa Chen, "Physical layer security in wireless networks: a tutorial," *IEEE Trans. Wireless Commun.*, vol. 18, pp. 66–74, 2011.

[4] M. Bloch and J. Barros, *Physical-Layer Security from Information Theory to Security Engineering*. Cambridge University Press, Oct. 2011.

[5] A. Babakhani, D. B. Rutledge, and A. Hajimiri, "Transmitter architectures based on near-field direct antenna modulation," *IEEE J. Solid- State Circuits*, vol. 43, no. 12, pp. 2674–2692, Dec. 2008.

[6] A. Babakhani, D. Rutledge, and A. Hajimiri, "Near-field direct antenna modulation," *IEEE Microw. Mag.*, vol. 10, pp. 36–46, 2009.

[7] A. H. Chang, A. Babakhani, and A. Hajimiri, "Near-field direct antenna modulation (NFDAM) transmitter at 2.4GHz," in *Antennas and Propagation Society International Symposium, 2009 IEEE*, 2009, pp. 1–4.

[8] M. P. Daly and J. T. Bernhard, "Directional modulation technique for phased arrays," *IEEE Trans. Antennas Propagat.*, vol. 57, pp. 2633–2640, 2009.

[9] M. P. Daly and J. T. Bernhard, "Beamsteering in pattern reconfigurable arrays using directional modulation," *IEEE Trans. Antennas Propagat.*, vol. 58, pp. 2259–2265, 2010.

[10] M. P. Daly, E. L. Daly, and J. T. Bernhard, "Demonstration of directional modulation using a phased array," *IEEE Trans. Antennas Propagat.*, vol. 58, pp. 1545–1550, 2010.

[11] H. Shi and T. Alan, "Direction dependent antenna modulation using a two element array," in *Proc. 5th Eur. Conf. on Antennas and Propagation*, 2011, pp. 812–815.

[12] H. Shi and T. Alan, "An experimental two element array configured for directional antenna modulation," in *Proc. 6th Eur. Conf. on Antennas and Propagation*, 2012, pp. 1624–1626.

[13] H. Shi and T. Alan, "Enhancing the security of communication via directly modulated antenna arrays," *IET Microw., Antennas Propag.*, vol. 7, no. 8, pp. 606–611, June 2013.

[14] Y. Ding and V. Fusco, "BER driven synthesis for directional modulation secured wireless communication," *International Journal of Microwave and Wireless Technologies*. Available: http://dx.doi.org/10.1017/S175-9078713000913

[15] Y. Ding and V. Fusco, "Directional modulation transmitter radiation pattern considerations," *IET Microw., Antennas Propag.* Available: http://dx.doi.org/10.1049/iet-map.2013.0282

[16] Y. Ding and V. Fusco, "Directional modulation transmitter synthesis using particle swarm optimization," in *Antennas and Propagation Conference (LAPC)*, Loughborough, UK, Nov. 11–12 2013, pp. 500–503.

[17] Y. Zhang, Y. Ding, and V. Fusco, "Sidelobe modulation scambling transmitter using Fourier Rotman lens," *IEEE Trans. Antennas Propagat.*, vol. 61, pp. 3900–3904, 2013.

[18] Y. Ding and V. Fusco, "Sidelobe manipulation using Butler matrix for 60 GHz physical layer secure wireless communication," in *Antennas and Propagation Conference (LAPC)*, Loughborough, UK, Nov. 11–12 2013, pp. 61–65.

[19] R. Negi and S. Goel, "Secret communication using artificial noise," in *Vehicular Technology Conference, 2005. VTC-2005-Fall. 2005 IEEE 62nd*, 2005, pp. 1906-1910.

[20] S. Goel and R. Negi, "Guaranteeing secrecy using artificial noise," *IEEE Trans. Wireless Commun.*, vol. 7, pp. 2180–2189, 2008.

[21] Y. Ding and V. Fusco, "A vector approach for the analysis and synthesis of directional modulation transmitters," *IEEE Trans. Antennas Propagat.* Available: http://dx.doi.org/10.1109/TAP.2013.2287001

[22] T. Hong, Mao-Zhong Song, and Y. Liu, "Dual-beam directional modulation technique for physical-layer secure communication," *IEEE Antennas Wireless Propag. Lett.*, vol. 10, pp. 1417–1420, 2011.

[23] C. A. Balanis, *Antenna Theory: Analysis and Design*, 3rd ed. New York: Wiley, 2005, pp. 27–29.

[24] N. Valliappan, A. Lozano, and R. W. Heath, "Antenna subset modulation for secure millimeter-wave wireless communication," *IEEE Trans. Commun.*, vol. 61, pp. 3231–3245, Aug. 2013.

[25] M. P. Daly, "Physical layer encryption using fixed and reconfigurable antennas," Ph.D. dissertation, Dept. Electrical and Computer Eng., University of Illinois at Urbana-Champaign, 2012.

[26] S. Forestier, P. Bouysse, R. Quere, A. Mallet, J.-. Nebus, and L. Lapierre, "Joint optimization of the power-added efficiency and the error-vector measurement of 20-GHz pHEMT amplifier through a new dynamic bias-control method," *IEEE Trans. Microw. Theory Techniques*, vol. 52, pp. 1132–1141, 2004.

[27] R. A. Shafik, S. Rahman, and AHM Razibul Islam, "On the extended relationships among EVM, BER and SNR as performance metrics," in *Proc. Int. Conf. on Electrical and Computer Engineering*, 2006, pp. 408–411.

[28] A. D. Wyner, "The wire-tap channel," *Bell Sys. Tech. Journ.*, vol. 54, no. 8, pp. 1355–1387, Oct. 1975.

[29] I. Csiszar and J. Korner, "Broadcast channels with confidential messages," *IEEE Trans. Inf. Theory*, vol. 24, pp. 339–348, 1978.

[30] Shunsuke Ihara, *Information Theory for Continuous systems*. World Scientific Publishing Co. Pte. Ltd., 1993, pp. 177–184.

[31] Ke-Lin Du and M. N. S. Swamy, *Wireless Communication Systems from RF Subsystems to 4G Enabling Technologies*. Cambridge University Press, 2010, pp. 571–575.

[32] G. Ungerboeck, "Channel coding with multilevel/phase signals," *IEEE Trans. Inf. Theory*, vol. IT–28, pp. 56–67, Jan. 1982.

[33] Philip Edward McIllree, 1995: Channel Capacity Calculations for M-ary N-dimensional Signal Sets. *M.E. thesis in Electronic Engineering*, The University of South Australia.

[34] J. P. Aldis and A. G. Burr, "The channel capacity of discrete time phase modulation in AWGN," *IEEE Trans. Inf. Theory*, vol. 39, pp. 184–185, Jan. 1993.

[35] C. E. Shannon, "A mathematical theory of communication," *Bell Syst. Tech. J.*, vol. 27, pp. 379–423, July 1948.

[36] Thomas M. Cover and Joy A. Thomas, *Elements of Information Theory*. 2nd ed. John Wiley&Sons, INC., 2006, pp. 261–264.

[37] A. H. Stroud, *Approximate Calculation of Multiple Integrals*. EnglewoodCliffs, New Jersey, Prentice-Hall, 1971, pp. 23–52.

[38] Vladimir Ivanovich Krylov (Translated by A. H. Stroud), *Approximate Calculation of Integrals*. Macmillan, New York, 1962, pp. 129–130 and pp. 343–346.

[39] S. T. Brink, "Convergence behavior of iteratively decoded parallel concatenated codes," *IEEE Trans. Commun.*, vol. 49, no. 10, pp. 1727–1737, Oct. 2001.

[40] Shunsuke Ihara, *Information Theory for Continuous systems*. World Scientific Publishing Co. Pte. Ltd., 1993, pp. 53–54.